University of Baghdad
College of Engineering
JE
JOURNAL OF ENGINEERING

Journal of Engineering

journal homepage: www.jcoeng.edu.iq

Volume 32 Number 1 January 2026

Frequency Dependence of Tension–Tension Fatigue in Woven Kevlar/Epoxy: Normalized S–N and Basquin Parameters at 0°, 23°, and 45°

Arzhang Faiq Mohammed *, **Kareem Abdulghafour Abdulla**

Department of Mechanical and Mechatronics Engineering, College of Engineering, Salahaddin University, Erbil, Kurdistan Region, Iraq

ABSTRACT

In this study, the combined effect of fiber orientation and loading frequency on tension–tension fatigue behavior of woven Kevlar/epoxy laminates was examined. Specimens with fiber orientations of 0°, 23°, and 45° were fabricated via hand lay-up and tested according to ASTM D3039 and ASTM D3479 standards. Static tensile tests with ultimate tensile strengths (UTS) of 276.1 MPa (0°), 159.2 MPa (23°), and 185.81 MPa (45°) showed clear orientation dependence. Fatigue stresses were normalized using (σ_{max}/UTS), Fatigue experiments were conducted at stress levels ranging from 55%to 90% of (UTS) and at two loading frequencies, 5 and 15 Hz. and the results were interpreted through normalized S–N curves, Basquin regression fits, ANCOVA, life reduction ratio (LRR), and SEM fractography. Increasing the loading frequency displayed reduced fatigue lives at all orientations. The 0° laminate experienced the most consistent frequency effect, with a mean LRR of 0.446 (95% CI: 0.381–0.511). In contrast, the 23° and 45° laminates showed smaller and more stress-dependent reductions, with mean LRR values of 0.186 (95% CI: 0.060–0.312) and 0.162 (95% CI: 0.041–0.284), respectively. ANCOVA results displayed no statistically significant frequency-induced slope differences ($p > 0.05$) for any orientation, indicating that the fatigue-life decay rate remained unchanged. However, intercept-level effects were practically large at 0° (partial $\eta^2 = 0.313$) and 23° (partial $\eta^2 = 0.229$), reflecting frequency-dependent reductions in fatigue strength. SEM observations also supported these observations, showing more extensive matrix cracking and fiber pull-out at higher frequency. Overall, woven Kevlar/epoxy laminates demonstrated strong anisotropic fatigue behavior, with fiber orientation serving as the dominant factor and frequency acting as a secondary yet influential parameter.

Keywords: Fiber orientation, Fatigue behavior, Frequency, Woven Kevlar

1. INTRODUCTION

Fiber-reinforced composites are widely used due to their high specific strength, stiffness, and favorable mechanical performance **(Reis et al., 2021)**. Laminated composites comprise

*Corresponding author
Peer review under the responsibility of University of Baghdad.
https://doi.org/10.31026/j.eng.2026.01.11

Article received: 30/09/2025
Article revised: 11/12/2025
Article accepted: 15/12/2025
Article published: 01/01/2026

stacked fiber–matrix layers, and their properties depend mainly on ply orientation, constituent materials, and stacking sequence **(Ahmed et al., 2023).** The research by **(Dehnad et al., 2022)** demonstrated that when fibers align with the loading direction, woven composites show fiber-dominated load transfer and high stiffness. **(Zhao et al., 2019)** reported that increasing fiber misalignment shifts failure from fiber-dominated to matrix-dominated modes due to higher shear deformation. Off-axis orientations reduce axial load-carrying capacity and accelerate damage accumulation, according to **(Ansari et al., 2022).** However, variations in weave architecture (fiber strength, density, twist, and inter-yarn bonding) make it difficult to identify a single precise off-axis angle that corresponds to minimum failure strength **(Li et al., 2025)**. In the laminate design must consider loading direction, ply orientation, and stacking sequence according to the expected axial or shear loads **(Bello et al., 2015).** The mechanical properties of fiber-reinforced composites with textile fabric reinforcements can be enhanced in directions of primary importance, generally in areas of highest stress concentrations **(Chowdhury and Summerscales, 2024)**. Compared to traditional unidirectional (UD) fiber reinforced composites, woven composites offer the added advantage of tuning the mechanical properties. This mechanical interlocking of fibers in two orthogonal directions in various weave patterns potentially leads to complex and interacting damage mechanisms **(Tewani et al., 2025).** Kevlar-reinforced composites are widely employed in demanding environments due to their high strength, toughness, and fatigue resistance **(Menail et al., 2015; Obradović et al., 2024; Reis et al., 2021)**. Kevlar is an aramid fiber of poly-para-phenyleneterephthalamide (PPTA)**,** where fibers are often used for high-performance composite applications where light weight, high strength and stiffness, damage resistance, and fatigue resistance are of utmost importance **(Prashanth et al., 2017; Rajesh et al., 2022)**. **(Salman et al., 2016)** investigated the tension-compression fatigue behavior of plain-woven Kenaf/Kevlar laminates and found damage accumulation and progressive stiffness loss, demonstrating that aramid fibers are sensitive to cyclic fatigue loading. Epoxy resins are highly versatile thermosets with excellent thermal and mechanical properties. They are widely used in coatings, adhesives, composites, insulation, and packaging materials **(Shundo et al., 2022).** Composite materials possess anisotropic properties, which lead to a more complex failure mechanism that mutually induce and couple with each other crucial aspect of various cyclic or highly dynamic loading conditions **(Yang et al., 2024)**. Therefore, understanding the characteristics of these composite materials under realistic service conditions is a crucial aspect of designing efficient and reliable products. However, the main load-bearing parts of structures made from composite materials experience various cyclic or highly dynamic loading conditions **(Ma et al., 2022)**. Evaluation of the fatigue behavior of composites under varied loading conditions is crucial to expand their usable range based on their advantages, such as superior drapeability, lower manufacturing costs, enhanced resistance to damage, and dimensional stability over a range of temperatures **(Schulte et al., 1987).** For this, extensive fatigue experiments for establishing an engineering fatigue failure prediction system that works for fabric composites under different fatigue loading situations are crucial for practically addressing this issue. Previous studies on the effect of loading frequency on laminated composites under tension–tension fatigue loading show mixed outcomes depending on fiber orientation and material type. For graphite/epoxy laminates, frequency had minimal influence, with only the 0° specimens showing slight sensitivity **(Justo Estebaranz et al., 2013; Marin et al., 2019)**. Transverse cracking studies on CFRP cross-ply laminates revealed that higher frequencies delayed crack initiation and

reduced propagation due to heat effects, although excessive heating could accelerate damage **(Deng et al., 2022)**. Studies on polyphenylene Sulfide (PPS)-Carbon Fiber (CF) and PPS-Glass Fiber (GF) laminates indicated that higher frequencies often reduced fatigue life due to self-heating, especially at off-axis orientations **(Růžek et al., 2018; Zuo et al., 2018)**. Similarly, advanced sheet molding compounds (A-SMC) and low-density sheet molding compounds (LD-SMC) showed drastic fatigue life reductions at very high frequencies (up to 40× shorter at 100 Hz) because of induced thermal fatigue **(Shirinbayan, 2021; Shirinbayan et al., 2017).** Fiber orientation plays a central role; fatigue life decreases as orientation approaches 90°, shifting failure from fiber- to matrix-dominated modes **(Ma et al., 2022)**. Small changes in frequency show limited effect, but higher frequencies may extend fatigue life unless overheating reduces durability **(Kawai and Taniguchi, 2006; Marin et al., 2019)**. For flax fiber composites, fatigue strength generally decreased with frequency, largely due to specimen temperature rise from internal friction **(Islam and Ulven, 2022)**.

Even though fatigue in composite laminates has been the subject of many investigations, little is known about how fiber orientation and loading frequency interact to influence fatigue performance under tension-tension loading, particularly in woven Kevlar/epoxy composites. The absence of consistent conclusions highlights a gap in knowledge that hinders the reliable design and application of Kevlar/epoxy laminates in structural components subjected to cyclic loads. The study aimed to use the experimental data, then analyze those data to evaluate the combined impact of fiber orientation and loading frequency on the fatigue behavior of laminated woven Kevlar/epoxy composites under tension–tension fatigue loading.

2. MATERIALS AND METHODOLOGY

This section describes the materials and fabrication process of composite laminates, as well as the testing procedures and analytical methods employed to characterize and interpret their tensile and fatigue behavior.

2.1 Test Coupons Fabrication and Preparation

Specimens were fabricated using the hand lay-up technique, and the typical fiber volume fraction ranges from approximately 30–40%. This range was employed for the specimens' fabrication. The tests were conducted in accordance with **(ASTM D3039/D3039M, 2008)** for tensile testing and **(ASTM D3479/D3479M, 2012)** for fatigue testing. **Table 1** lists the Mechanical and physical specifications (Tensile Strength (S), Tensile Modulus (E), and density (ρ)) of the Kevlar fibers and the matrix material used in the study.

Table 1. Specifications of the woven Kevlar fiber with epoxy**.**

Elements	S(MPa)	ρ(g/cm^3)	E(GPa)	Type
Kevlar Fiber	≥ 2400	1.45	≥ 90	TWARON 930DTEX_WRAP/WEFT
Epoxy Resin + Hardener	60	1.15	3	LR-620 epoxy+H620 hardener

A seven-layer symmetric lay-up was prepared for all laminates, with woven Kevlar fabric oriented at 0°, 23°, or 45° depending on the test group. Each layer was impregnated manually using LR-620 epoxy and H620 hardener at the manufacturer-recommended mixing ratio, ensuring full resin wet-out before stacking. The laminate was consolidated using hand lay-up with a uniform roller to remove entrapped air and achieve a consistent fiber volume

distribution, and before curing the sheet was put under vacuum to remove the air trapped as much as possible. A graphical representation (flow chart) of the step-by-step hand-layup fabrication process for laminated composites is provided in **Fig. 1.** The composite sheets were trimmed to standard dimensions under ASTM D3039 and ASTM D3479 standard dimensions after manufacture, and the samples were identical for the static and fatigue tests, with a rectangular cross-section of 44 mm^2, and dimensions of (length, breadth, thickness), with desired fiber orientations ∅ as presented in **Fig. 2**.

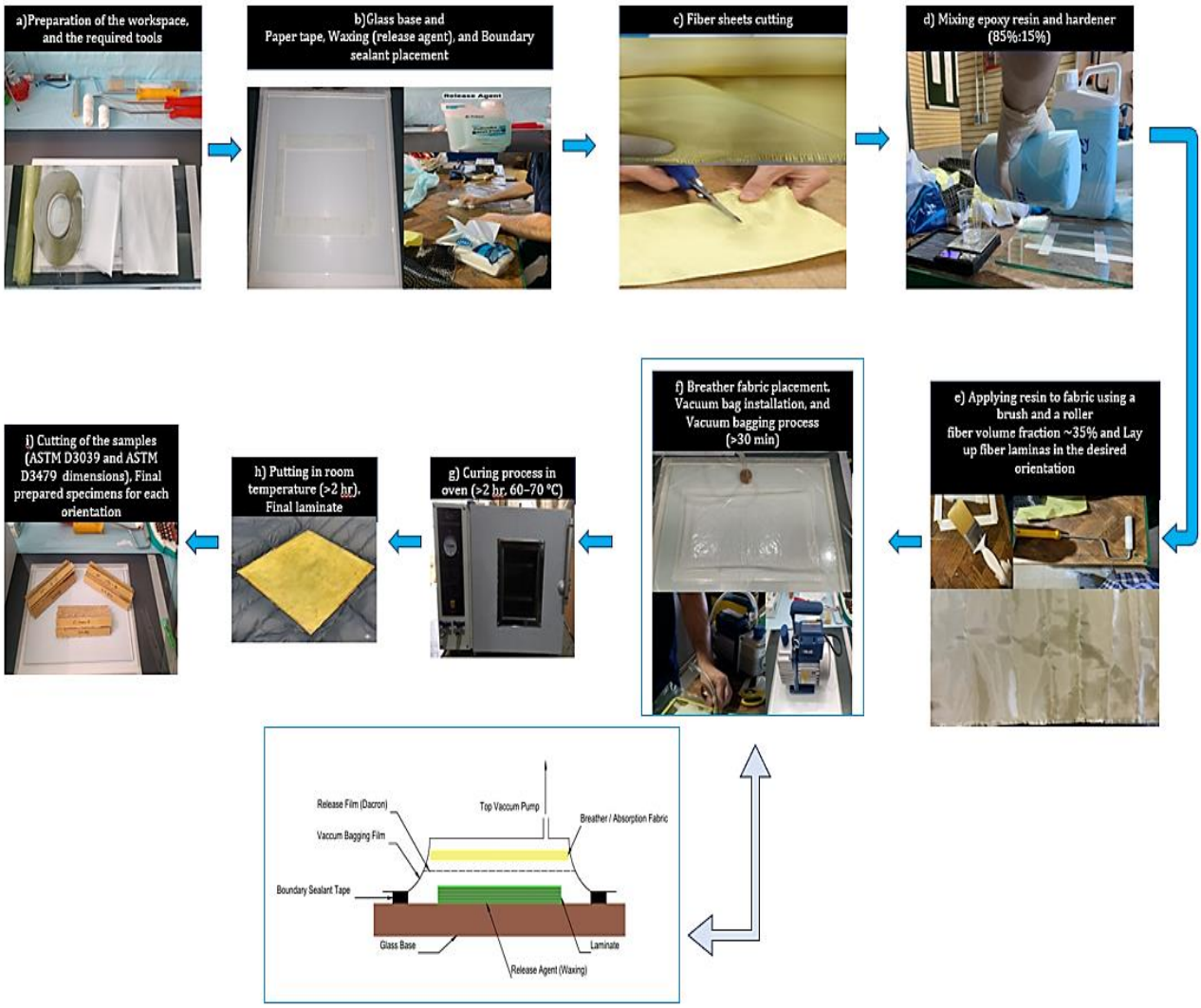

Figure 1. Graphical representation of the step-by-step hand-layup fabrication process of the laminated composites.

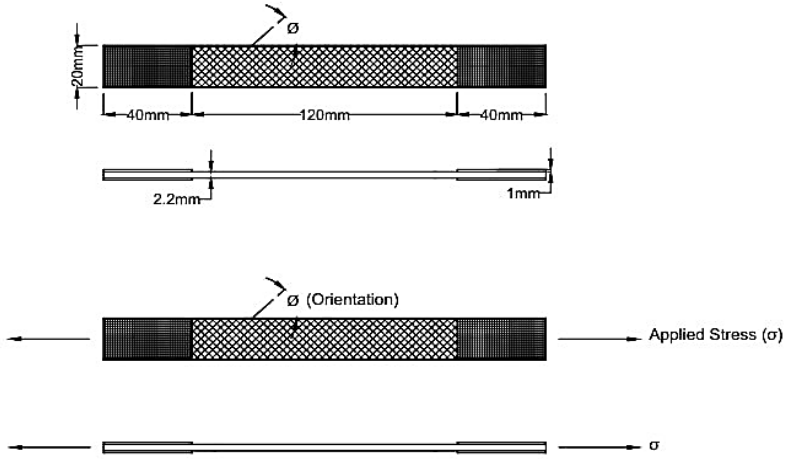

Figure 2. The test specimen dimensions and schematic of fiber orientation (Ø) with respect to the loading direction (σ) for the 0°, 23°, and 45° laminates.

2.2 Testing Methodology

2.2.1 Uniaxial Tensile Testing

An SANTAM STM-250 Hydraulic testing machine located in the Materials Testing Laboratory at Urmia University was used to perform static tensile tests at room temperature, with displacement regulated at a rate of 0.5 mm/min. The static test was intended to determine the maximum tensile strength that the specimens could withstand at each fiber orientation. For each orientation, the average ultimate tensile strength (UTS) was calculated from three woven Kevlar/epoxy specimens tested under static loading. For the static tensile test, **(ASTM D3039/D3039M, 2008)** was utilized as a reference. The end tabs were made from 1-mm aluminum sheets and bonded using a two-part epoxy adhesive in accordance with **(ASTM D3039/D3039M, 2008).** Specimen alignment and bending strain were verified using a two-sided Digital Image Correlation (DIC) system capturing synchronized strain fields on both faces of the specimen, confirming bending levels within the **(ASTM D3039/D3039M, 2008)** limit of 10%. The stress levels for the dynamic fatigue tests were determined by calculating the UTS and expressing it as a percentage of the maximum strength.

2.2.2 Tension-Tension Fatigue Testing

Fatigue tests were performed using a Dartec servo-hydraulic fatigue testing machine, located in the Materials Testing Laboratory at Amirkabir University of Technology (Tehran Polytechnic). The system is equipped with controlled loading capabilities and adjustable frequency settings, enabling precise application of dynamic cyclic loading. A sinusoidal tension–tension loading function with a maximum load capacity of 50 kN, a maximum operating frequency of 100 Hz, and the stress ratio presented in Eq. (1)**,** remained constant for all tests (R = 0.1) was employed, ensuring that frequency was the only variable affecting the cyclic loading conditions. Tests were performed under controlled laboratory temperature with continuous airflow, following **(ASTM D3479/D3479M, 2019)** standard recommendations.

$$R = \frac{\sigma_{\min}}{\sigma_{\max}} = 0.1 \quad (1)$$

where σ_{max} is the maximum stress and σ_{min} is the minimum stress applied.

Based on a percentage of the UTS determined from the static tests, the stress levels were established, which varied from 90% to 55% of the UTS, for reference. These thresholds have been selected because they cover stress levels corresponding to the high- and low-stress fatigue regimes that are frequently employed in composite fatigue testing, while 55% UTS is associated with long-life, high-cycle behavior, the high stress levels 90% UTS represent low-cycle fatigue. The tests were done at frequencies (5 Hz and 15 Hz) to assess the loading frequency effect. A run-out limit of 10^6 cycles was adopted. Specimens that reached this limit without failure were classified as run-outs and treated as right-censored observations
In the fatigue analysis, finally, for every test scenario, the number of cycles until failure was recorded.

2.3 Fatigue Data Interpretation Methods and Statistical Analysis

2.3.1 Normalized S–N, Basquin, and ANCOVA Analysis

To allow direct comparison of the frequency effect across all orientations, fatigue stresses were normalized with respect to the ultimate tensile strength (UTS) as expressed in Eq. (2), as recommended by composite fatigue testing **(ASTM D3479/D3479M, 2012).**

$$\sigma_{\text{norm}} = \frac{\sigma_{\max}}{\text{UTS}} \tag{2}$$

Six normalized stress levels (55–90% UTS) were applied to each laminate (0°, 23°, 45°) at two loading frequencies (5 Hz and 15 Hz). The resulting cycles-to-failure data were transformed using $\log_{10}(N)$ and plotted against (σ_{norm}) to draw the Normalized S–N curves for each orientation and frequency. The use of log–log S–N representation and stress normalization follows conventional fatigue analysis **(Bannantine et al., 1990; Suresh, 1998)**
The fatigue behavior was quantified using Basquin's law, expressed in Eq. (3), because it provides a widely phenomenological model for fatigue in fiber-reinforced polymer composites, enabling linear log–log regression between stress amplitude and fatigue life and facilitating the comparison of frequency-dependent fatigue behavior. **(Basquin, 1910; Suresh, 1998).** The analysis followed the conventional S-N methodology outlined by **Bannantine et al., 1990)** who describe the use of Basquin's power-law relation and the linear regression procedures commonly applied to log–log fatigue data**.**

$$\sigma_{\max} = A.N^{-b} \tag{3}$$

where A is the fatigue-strength coefficient in MPa, and b is the fatigue exponent, which can be determined using Eqs. (4) and (5), respectively, and $\sigma_{\max}$ is the maximum permissible stress in MPa.

$$A = 10^{\text{C}} \tag{4}$$

$$log(\sigma_{max}) = c - b.\log(N) \tag{5}$$

Where, c is the intercept**.**
Linear regression was applied to each dataset (orientation × frequency) to determine the slope (b) and intercept (c), along with standard errors (SE), 95% confidence intervals (95% CI), and the coefficient of determination R^2 **(Montgomery et al., 2021)**

To obtain orientation-independent comparisons, the fatigue strength coefficient was also normalized as expressed in Eq. (6) **(ASTM D3479/D3479M, 2012).**

$$A_{\text{norm}} = \frac{A}{\text{UTS}} \tag{6}$$

ANCOVA was applied to compare the Basquin-derived fatigue slopes and interceptions between 5 Hz and 15 Hz for each orientation. The full model tested slope differences using the interaction term in Eq. (7) **(Montgomery et al., 2021; Wickens and Keppel, 2004)**

$$logN = \beta_0 + \beta_1 log\sigma + \beta_2 f + \beta_3 (log\sigma \times f) + \epsilon \tag{7}$$

A non-significant interaction ($p > 0.05$) indicated slope equivalence. When slopes were parallel, a reduced model assessed intercept differences as expressed in Eq. (8) **(Wickens and Keppel, 2004)**

$$\log(N) = \beta_0 + \beta_1 \log(\sigma) + \beta_2 f + \epsilon \tag{8}$$

where log (N) represents the logarithm of cycles to failure, log (σ) denotes logarithm of maximum stress, f is frequency (categorical: 0 = 5 Hz, 1 = 15 Hz), β_0 stands for the intercept, β_1 is the Basquin slope at the reference frequency (5 Hz), β_2 is intercept shift due to frequency, β_3 is the change in slope due to frequency (interaction term),ϵ is residual error term, Effect-size thresholds for partial η^2: small (<0.06), medium (0.06−0.14), large (≥0.14) follow the guidelines summarized by **(Richardson, 2011)**, based on **(Cohen, 1988)**.

2.3.2 Frequency Comparison Using LRR

The influence of loading frequency on fatigue performance was quantified using the life reduction ratio LRR ($1 - \frac{N_{15}}{N_5}$)where N_5 and N_{15} represent the number of cycles to failure obtained at test frequencies of 5 Hz and 15 Hz, respectively, under the same normalized maximum stress level ($\sigma_{\max}$/UTS). LRR was evaluated at six stress levels ranging from 90% to 55% of UTS for each orientation (0°, 23°, and 45°).

For each orientation, six LRR values (one per stress level) were used to compute the mean LRR and its corresponding standard error (SE). The 95% confidence interval (95% CI) was determined using the Student's t-distribution with five degrees of freedom (df = 5). The corresponding %LRR values (LRR × 100) were reported in the summary table for interpretational clarity. This procedure provides a normalized, orientation-independent method for comparing fatigue life between the two test frequencies.

2.3.3 SEM Failure Mode Analysis

Scanning electron microscopy (SEM) was used to examine the fracture surfaces of the specimens after fatigue failure. The SEM inspection focused on identifying dominant failure features, including matrix cracking, fiber/matrix debonding, fiber pull-out, breakage, and overall fracture morphology. SEM analysis was performed mainly on specimens tested at 55% UTS because the failure modes at different frequencies could be better captured by these samples, which had the most cycles to failure, as their longer fatigue lives enabled clearer visualization of frequency-dependent damage characteristics.

3. RESULTS AND DISCUSSION

This section summarizes the static and fatigue results and includes statistical analyses to evaluate the effects of fiber orientation and loading frequency on the mechanical behavior of the composites.

3.1 Static Results

The mechanical performance of Kevlar/epoxy woven laminates was greatly affected by fiber orientation, as demonstrated by the average stress-strain curves in **Fig. 3** at 0°, 23°, and 45°. When the fibers were parallel to the loading axis, the laminate exhibited the sharpest stress-strain response at 0°, indicating a very high elastic modulus. Since the tensile load and the reinforcing yarns were aligned in the same direction, this can be explained by the load acting directly on them at this angle. Additionally, this orientation has the highest ultimate tensile strength, indicating the increased strength generated by fiber-dominated load transfer. However, as **Table 2** shows, this alignment has a very limited strain capacity and fails suddenly at low strain levels, unlike the other orientations. The fibers exhibit brittle-like behavior.

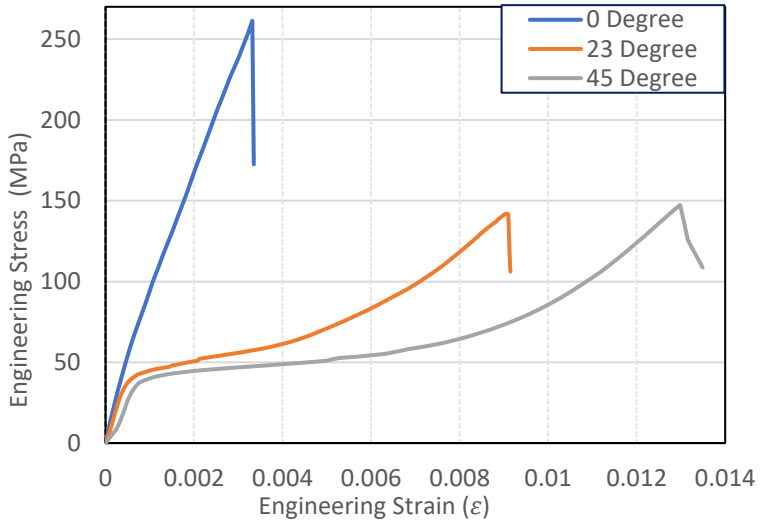

Figure 3. Avg Stress-Strain curve of the woven Kevlar/epoxy samples at different fiber orientations.

Table 2. Summary of the average tensile modulus (E_{avg}), ultimate tensile strength (UTS_{avg}), and engineering strain at UTS (ε_{avg}), together with their corresponding standard deviations (E_{std}, UTS_{std}, ε_{std}), for woven Kevlar/epoxy laminates at fiber orientations of 0°, 23°, and 45°.

Orientation	E_{avg} (GPa)	E_{std} (GPa)	UTS_{avg} (MPa)	UTS_{std} (Mpa)	ε_{avg}	ε_{std}
0°	58.0	12.4	276.1	8.2	0.0036	0.0004
23°	9.8	2.7	159.2	4.5	0.0098	0.0010
45°	6.0	0.8	185.8	1.8	0.0146	0.0020

At 23°, there is a noticeable change in the laminate's reaction. In comparison to 0°, the stiffness and ultimate strength decrease because the fibers are not aligned to directly withstand the applied force. Rather, the matrix transfers a greater proportion of the stress through shear interactions between the fibers and resin. Although the strength has

decreased, more deformation before failure is granted. The strain at the final stress was significantly higher than at 0°, indicating that a more intricate failure occurred at 23° orientations. This is because of the transition zone, indicating a transition from fiber-dominated to matrix-dominated failure. where both off-axis and on-axis failure modes have been occurring in the 23° off-axis specimens. At a 45° angle, the most compliant response was seen. The orientation with the lowest modulus among those analyzed was indicated by the curve's shallow starting slope. In off-axis laminates, the load is mostly carried by shear in the fiber/matrix interface due to the fibers being totally out of alignment with the loading axis, which results in limited axial strength and rapid degradation of the composite. However, the composite can sustain the largest strain before failing since the curve spans the widest strain range. This illustrates a shear-dominated deformation mechanism in which matrix plasticity, fiber shear, and growing micro-damage allow the material to stretch significantly. After peak stress, the failure mechanism is more ductile-like and softens gradually, in contrast to the 0° specimens that ruptured quickly. The UTS of a 45-degree orientation fell between 0 and 23 degrees. Since the fibers at 23° are not properly oriented for axial load or balanced shear, the performance of woven laminates depends on matrix shear, fiber rotation, and debonding, and due to this dependability in the woven laminates, it is difficult to identify a specific off-axis angle that consistently corresponds to the minimum failure strength. On the other hand, the failure strain rises proportionately with the off-axial angle, peaking at 45°.

3.2 Fatigue Results

Fatigue stresses were normalized using (σ_{max}/UTS), and the results were evaluated using normalized S–N curves, Basquin regression, ANCOVA, LRR, as well as SEM. Basquin parameters, ANCOVA p-values and effect sizes, and LRR statistics are summarized in **Tables 3 to 5.**

3.2.1 Normalized S-N and Basquin Curve Fits Assessments

Fig. 4(a-c) displays the normalized S–N diagrams (σ_{max}/UTS vs Log(N)) for the laminated composites of all orientations with Basquin's fitted lines at 5Hz and 15Hz loading frequencies. Each S–N plot shows individual data points and fitted Basquin lines, and the 95% confidence intervals for the Basquin parameters are reported in **Tables 3 to 4**.

The graph for the 0° laminate with Basquin fitted lines, displayed in **Fig. 4(a),** showed that the two fitted lines were almost parallel (with Similar slopes, b = 0.098) for 5 Hz and 15 Hz frequencies. This indicates that the fatigue degradation rate was constant at both frequencies. However, the downward vertical shift of the 15 Hz fitted line indicates reduced normalized fatigue strength, and this indicates that increasing Frequency mostly reduces fatigue strength without changing the sensitivity to fatigue-life and stress levels.

At 23° orientation, the fatigue response of the woven Kevlar/epoxy laminate showed sensitivity of the laminate to loading frequency and fiber orientation. The lower intercept in relation to 0° indicates decreased fatigue strength compared to the 0° laminates. Basquin's fits had steeper slopes (b= 0.196 at 5 Hz and 0.178 at 15 Hz). These slopes indicate that the separation between the two fitted lines is not constant; it is large in the high-stress region and gradually decreases as the stress level reduces. Although the 15 Hz curve's degradation patterns consistently exhibit a persistent leftward offset relative to the 5 Hz curve for all tested stress levels, indicating that the 23° laminate has less endurance at higher

frequencies. The S-N graph of the 23° laminate with its Basquin fits at 5Hz and 15Hz frequencies is shown in **Fig. 4(b).**

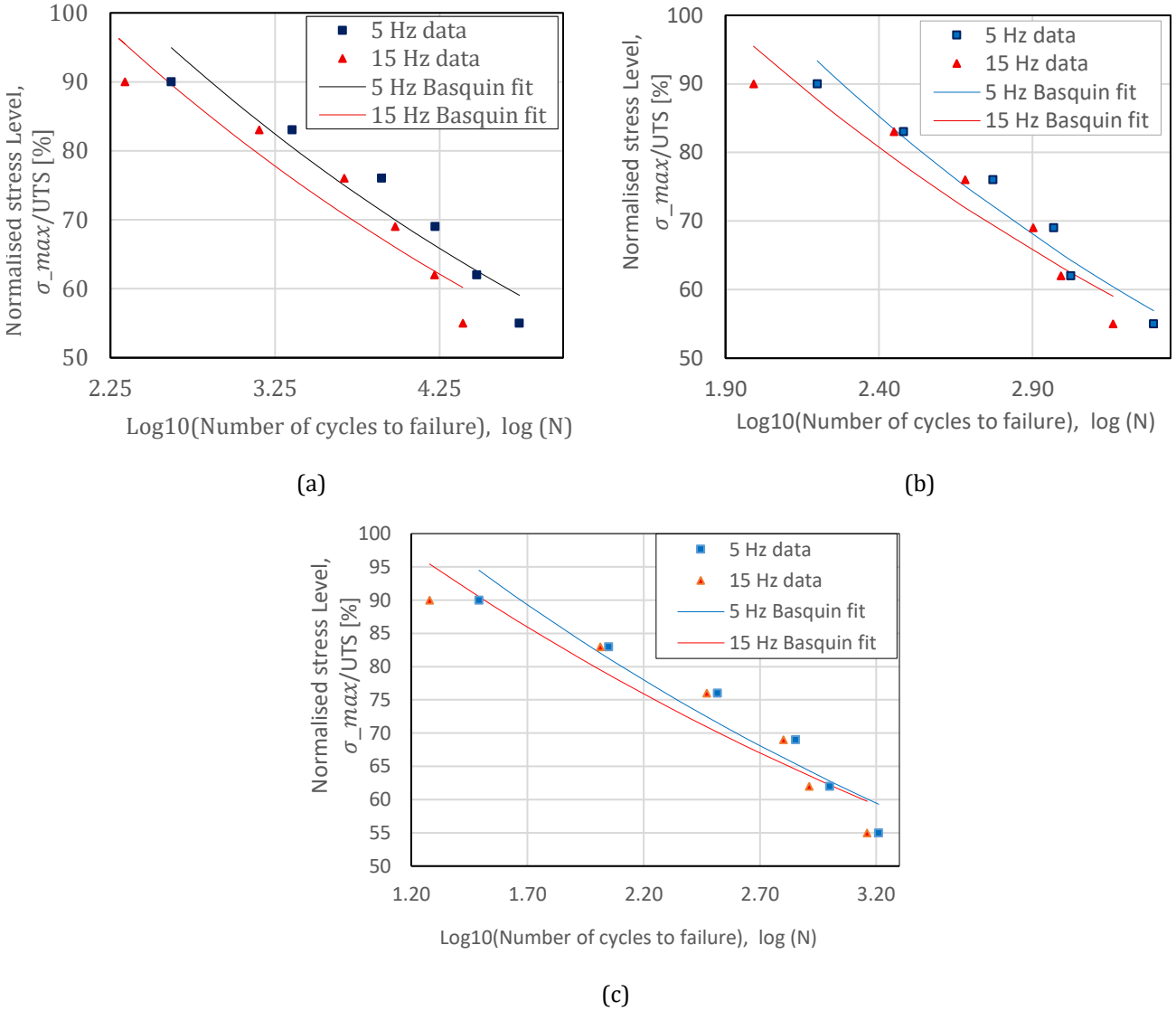

Figure 4. Normalized S–N curves with Basquin fits for woven Kevlar/epoxy laminates at fiber orientations of (a) 0°, (b) 23°, and (c) 45°.

The 45° laminate demonstrated less fatigue resistance than both the 0° and 23° orientations since it had lower intercepts than 0° and 23°. The 45° Basquin fits' slopes (0.118 at 5 Hz and 0.108 at 15 Hz) were slightly greater than the 0° slopes, but they were still considerably fewer than the 23° laminate's slopes, as shown in **Fig. 4(c).**

The 15 Hz Basquin line remained consistently lower than the 5 Hz line. At 15 Hz, the 45° laminate likewise exhibited decreased normalized strength, but with a smaller separation than the 0° and 23° laminates, demonstrating that increased frequency reduces fatigue strength. However, the reduction at 45° was smaller than the reduction at 23°, and considerably smaller than the reduction observed for the 0° laminate, which showed the largest and most uniform frequency effect. However, for the 0° laminate, the frequency effect was nearly constant across all stress levels, with a similar 5–15 Hz separation at both high

and low stresses, while the 23° and 45° laminates showed a reduction in the frequency effect at lower stress levels.

3.2.2 Basquin Regression Parameters

The Basquin regression and fatigue strength parameters are listed in **Tables 3 and 4**, respectively. They quantify the trends observed in the normalized S–N diagrams and describe how frequency and orientation influence the stress–life relationship. Basquin coefficients (b and c) define the slope and position of the normalized S–N curves, while the fatigue strength parameters (A and A_{norm}) directly measure the effective fatigue endurance at each orientation and frequency. These parameters (b, c, A, A_{norm}, SE, and R^2) offer a concise statistical summary of the stress–life behavior for each orientation and frequency.

The Basquin fits with identical slopes (b) (0.098 for both frequencies) at 0°, moderate difference (0.196 vs 0.178) at 23°, and small difference (0.118 vs 0.108) at 45° laminates, indicating that in all orientations, the slope is relatively insensitive to frequency, indicating that the rate at which fatigue life decreases per log cycle of stress is not strongly influenced by cyclic frequency.

Both the intercept (c) and the fatigue strength coefficient (A) show the same orientation-dependent trend in how frequency affects fatigue strength. When the loading frequency increases from 5 Hz to 15 Hz, the 23° laminate exhibited the largest reduction in both normalized intercept ($\Delta c = 0.066$) and absolute fatigue strength ($\Delta A = 57$ MPa, -14.2%), the 45° laminate with a moderate reduction ($\Delta c = 0.033$, $\Delta A = 19$MPa, -7.2%), and the 0° laminate displayed the smallest reduction ($\Delta c = 0.025$, $\Delta A = 26$MPa, -5.5%) indicating that the 0° laminate experiences the smallest reduction in fatigue strength when frequency increases, with only a minimal change in the vertical position of its S–N curve, while the 23° and 45° laminates, on the other hand, show greater decreases, indicating higher frequency sensitivity in terms of fatigue strength.

Table 3. Basquin Regression Parameters (b, c, SE, 95% CI, R^2)

Orientation (°)	Freq (Hz)	Slope (b)	SE(b)	95% CI (b)	Intercept (c)	SE(c)	95% CI (c)	R^2
0	5	0.098	0.015	0.056-0.139	2.674	0.059	2.509-2.839	0.91
0	15	0.098	0.018	0.047-0.148	2.649	0.067	2.463-2.836	0.88
23	5	0.196	0.023	0.132-0.26	2.603	0.065	2.424-2.782	0.95
23	15	0.178	0.029	0.097-0.26	2.537	0.08	2.314-2.759	0.9
45	5	0.118	0.019	0.066-0.169	2.42	0.048	2.287-2.553	0.91
45	15	0.108	0.02	0.052-0.164	2.387	0.05	2.247-2.527	0.88

Table 4. Fatigue Strength Parameters (A, A_{norm}, 95% CI)

Orientation (°)	Freq (Hz)	A (MPa)	95% CI A(MPa)	A_{norm} (%UTS)	95% CI (A_{norm})
0	5	472	323.1-690.2	1.71	1.17-2.5
0	15	446	290.4-684.7	1.62	1.05-2.48
23	5	401	265.4-605.7	2.52	1.67-3.8
23	15	344	206.3-574.5	2.16	1.3-3.61
45	5	263	193.6-357.3	1.42	1.04-1.92
45	15	244	176.5-336.6	1.31	0.95-1.81

The R^2 values range from 0.88 to 0.95 across all cases, demonstrating consistently strong linearity and validating the reliability of the Basquin model for this system. With R^2 (0.95), the 23° laminate at 5 Hz exhibited the best fit. Finally, overlapping 95% CI shows that while the intercepts and fatigue strength coefficients decrease with increasing frequency, these decreases are not statistically significant, indicating qualitative patterns consistent with the inherent variability of composite fatigue data.

3.2.3 ANCOVA Findings

ANCOVA was used to compare slopes and intercepts between 5 Hz and 15 Hz, with both p-values and partial η^2 are reported to quantify frequency effects. **Table 5** displays the ANCOVA results. The results showed several points: i) frequency did not produce a statistically significant difference in the Basquin slopes for any orientation ($p > 0.05$). This confirms that the rate of fatigue-life decay per stress level remained essentially unchanged between 5 Hz and 15 Hz. ii) the intercepts exhibited large practical (effect-size) differences at 0° (η^2 = 0.313) and 23° (η^2 = 0.229), indicating meaningful frequency-induced reductions in overall fatigue-life levels, despite the absence of statistical significance iii) The 45° laminate showed only a small practical effect (η^2 = 0.055), consistent with its lower LRR values. iv) Collectively, these results indicate that frequency primarily influences the intercept (fatigue-life magnitude) rather than the slope (fatigue-life decay rate), with the strongest practical effects occurring in the 0° and 23° orientations.

Table 5. ANCOVA results for (b) and (c) differences between 5 Hz and 15 Hz per orientation.

Orientation	Effect	p-value	partial η^2	Interpretation
0	Slope	0.978	0.0001 (Negligible)	Slopes identical
0	Intercept	0.074	0.313 (Large)	Large practical effect
23	Slope	0.595	0.037 (Small)	Slopes identical
23	Intercept	0.136	0.229 (Large)	Large effect
45	Slope	0.677	0.023 (Small)	Slopes identical
45	Intercept	0.488	0.055 (Small)	Small effect

3.3 LRR Evaluation

The LRR values obtained for the three orientations provide a quantitative basis for comparing the fatigue lives measured at 5 Hz and 15 Hz at different stress levels. the mean LRR, SE, and 95% CI are listed in **Table 6**. The 0° laminate displayed the largest and most uniform mean LRR (0.446) across the stress range of 55–90% UTS, with a relatively narrow 95% CI of 0.381–0.511. This indicates that the fatigue-life difference between the two frequencies was consistent for this orientation across all stress levels. Lower mean LRR values of 0.186 (95% CI: 0.060–0.312) and 0.162 (95% CI: 0.041–0.284) were obtained for the 23° and 45° laminates, respectively, reflecting smaller differences in fatigue life between the two frequencies compared with the 0° orientation. The broader 95%CI for the 23° and 45° laminates indicates greater variability in LRR across the examined stress levels. At σ_{max}= 90% UTS, the LRR values were 0.48 (0°), 0.38 (23°), and 0.39 (45°). At mid-range stresses (69–76% UTS), the LRR values decreased to approximately 0.14–0.19 for 23° and 0.10–0.11 for 45°, while remaining comparatively stable for the 0° orientation. These results display that frequency-induced life reduction was largest and most uniform for the 0° laminate, moderate and concentrated at high stresses for the 23° laminate, and smallest for the 45° laminate.

Table 6. Summary of Mean LRR, standard error (SE), %LRR, and 95% CI for each orientation.

Orientation	LRR (mean)	SE (LRR)	%LRR (mean)	95% CI (LRR)
0°	0.446	0.025	44.6	0.381-0.511
23°	0.186	0.049	18.6	0.060-0.312
45°	0.162	0.047	16.2	0.041-0.284

3.4 SEM Results and Failure Modes

Utilizing SEM, the morphological properties of the laminated woven Kevlar/epoxy composites were examined. These images demonstrate the main microstructural characteristics and damage trends associated with the woven structure under various fatigue loading scenarios. The SEM observations revealed damage mechanisms that are widely documented in composite laminates, including matrix microcracking, fiber–matrix debonding, fiber pull-out, and layered fracture morphology **(Liu et al., 2025; Mohammadi et al., 2024; Opelt et al., 2018).**

Figs. 5 to 7 display the comparable SEM micrographs for the 0°, 23°, and 45° laminates at 5 Hz and 15 Hz. In general, the SEM images showed that a fibrillated and layered Kevlar fracture was regularly seen at both frequencies and in every orientation. Higher frequency (15 Hz) resulted in more fiber pull-out and matrix debris, along with macrocracks and voids from concentrated stress. Both the 5 Hz and 15 Hz experiments revealed fibrillated fracture surfaces at 0° orientation; however, the higher frequency resulted in more obvious matrix debris and short-fiber pull-out, while the surface at 5 Hz was primarily covered by scattered short fibers clear of debris. Significant long-fiber pull-out together with scattered matrix fragments at 15 Hz indicated more severe fiber–matrix separation, whereas 5 Hz samples showed a random dispersion of short and long fibers at 23° orientation. In the 45° orientation, a similar pattern appeared. While 5 Hz testing revealed scattered short fibers, 15 Hz testing revealed increased damage with wider breaks and both short and long chaotic fibers. No delamination occurred in either direction or frequency, indicating that the damage was confined to the Kevlar yarns rather than spreading across layers.

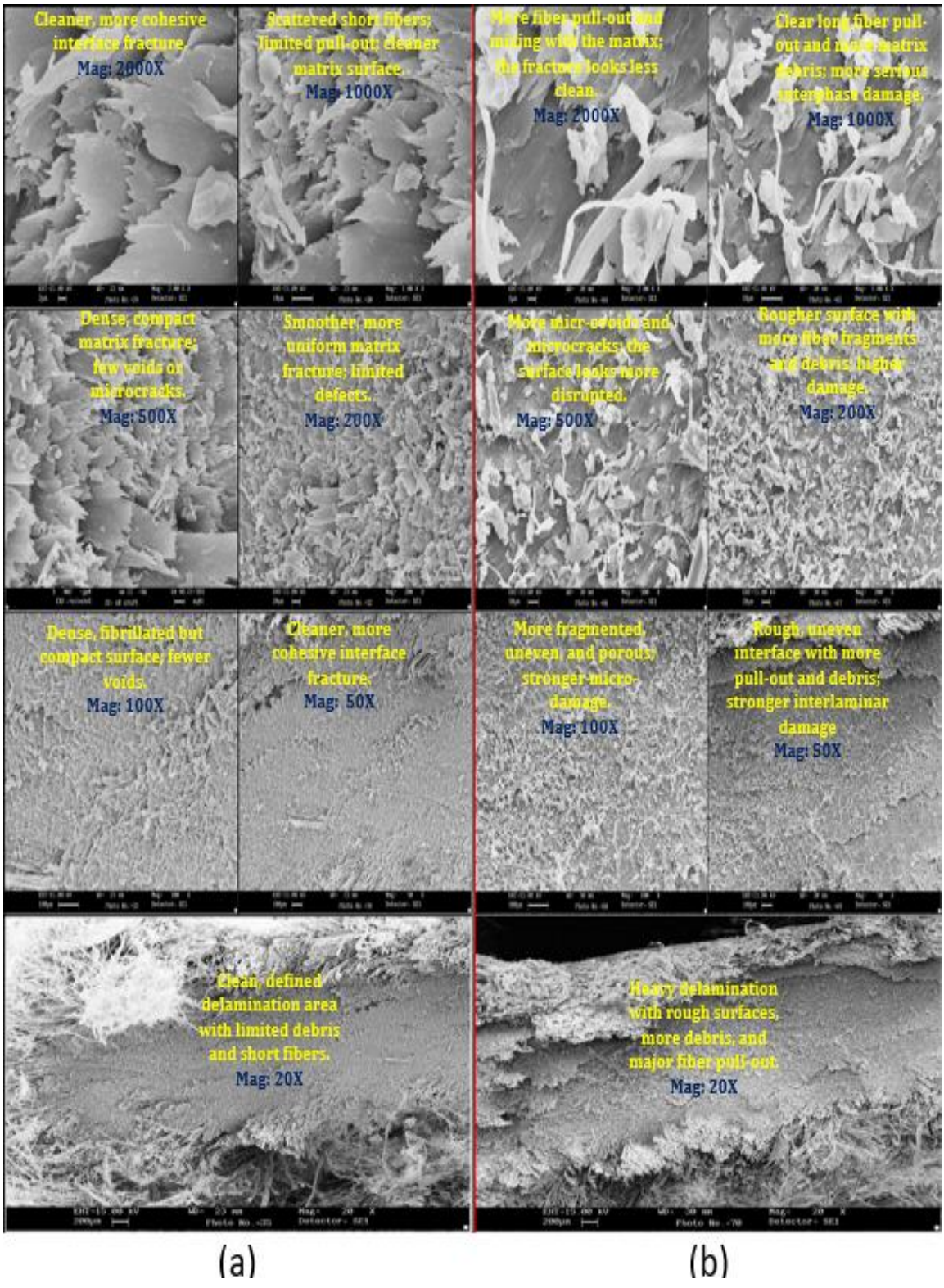

Figure 5. SEM results for 0° laminate a) failure at 5Hz, and b) failure at 15Hz at different magnification scales

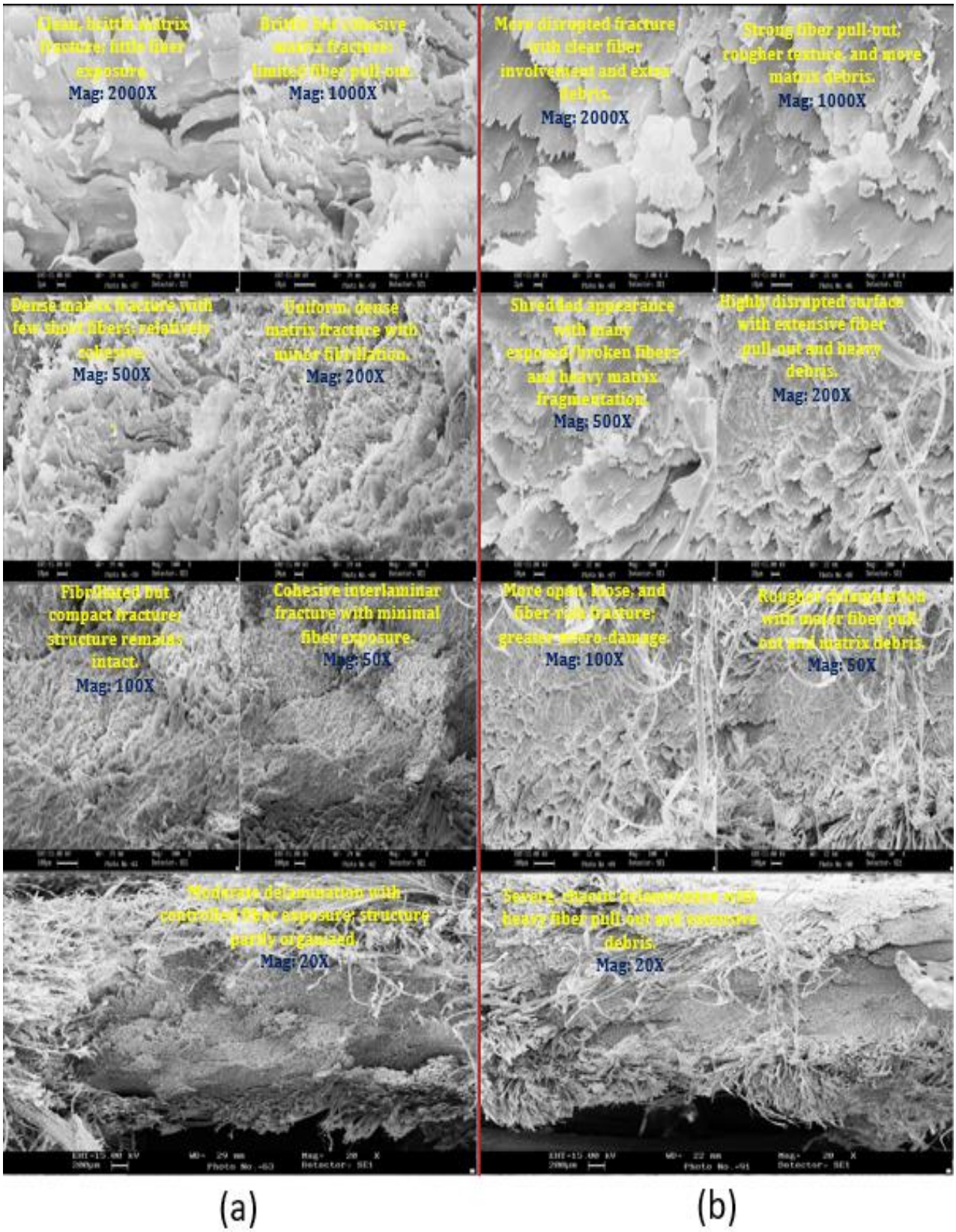

Figure 6. SEM results for 23° laminate a) failure at 5Hz, and b) failure at 15Hz at different magnification scales

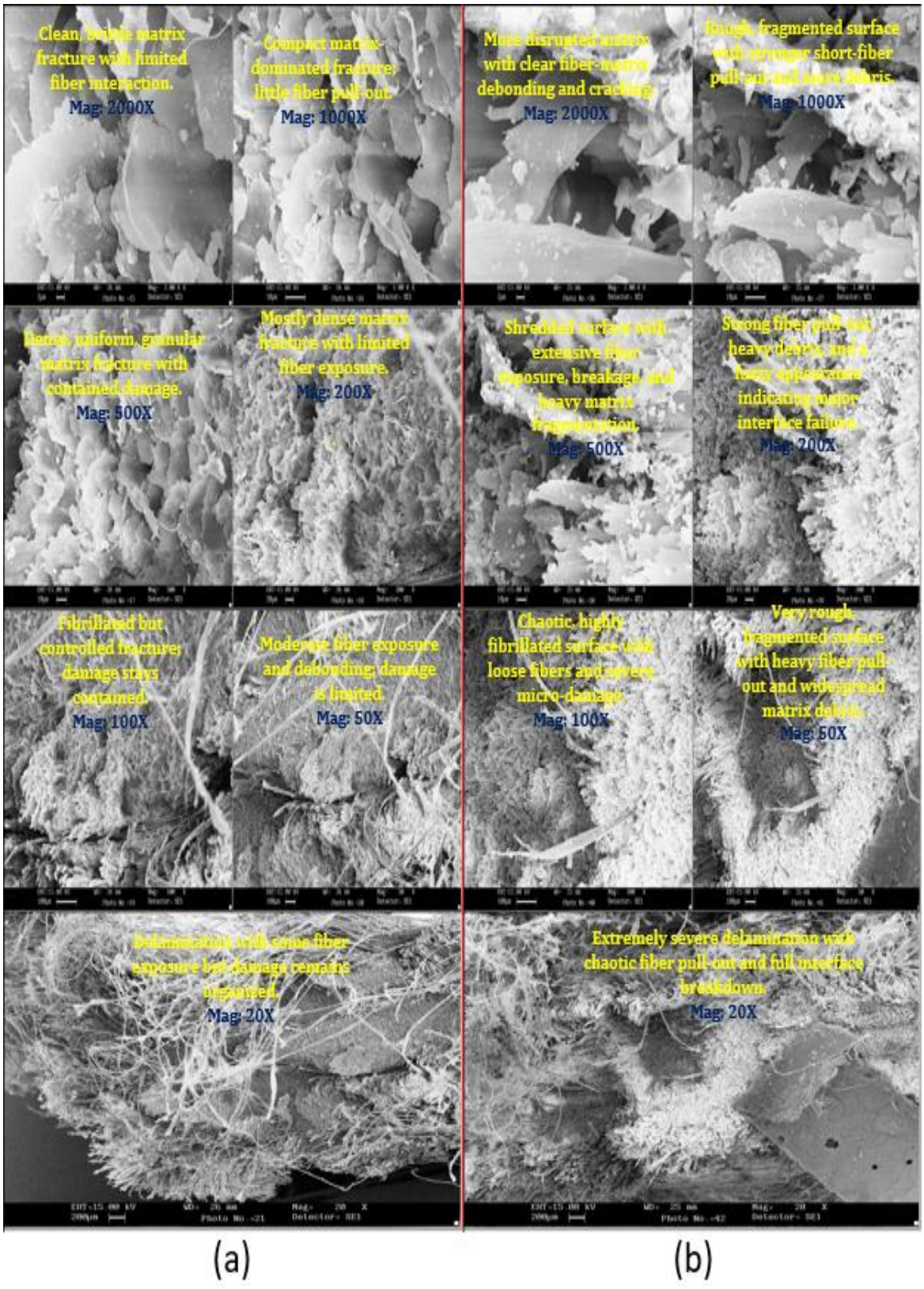

Figure 7. SEM results for 45° laminate a) failure at 5Hz, and b) failure at 15Hz at different magnification scales

4. CONCLUSIONS

The combined effects of loading frequency and fiber orientation on the tensile and fatigue response of woven Kevlar/epoxy laminates were evaluated in this study using normalized S–N curves, Basquin regression, ANCOVA, LRR evaluation, and SEM fractography. Results show that both orientation and frequency influence the fatigue strength and damage behavior of the laminates.

- The 0° laminate exhibited the highest static and fatigue capacities, followed by the 23° and 45° laminates.
- Normalized S–N curves supported this classification, and Basquin parameters further demonstrated the orientation dependence: the 23° laminate had the largest slopes, indicating the highest sensitivity to stress level, while the 45° laminate demonstrated the lowest fatigue strength among the tested orientations.
- All specimens failed before the run-out threshold (10^6 cycle), so no right-censored data were generated in the study.
- The effect of frequency showed vertical shifts in the normalized S–N curves rather than changes in slope, and ANCOVA statistics agreed with that by showing that increasing the frequency did not significantly alter the fatigue-life decay rate for any orientation.
- However, reductions in interceptions revealed decreased fatigue strength at higher frequency, with large practical effects at 0° and 23°, and a smaller effect at 45°.
- Basquin fits showed strong linearity (R^2 values range from 0.88 to 0.95 across all cases).
- LRR analysis supported these trends: the 0° laminate showed the largest and most uniform life reduction, while the 23° and 45° laminates exhibited smaller and more stress-dependent reductions.
- SEM observations showed more extensive matrix debris, fiber pull-out, and surface fragmentation at 15 Hz, consistent with the measured reductions in fatigue strength.
- Although specimen temperature was not recorded, prior studies suggest that self-heating at higher frequencies may contribute to the observed reductions in fatigue strength.

Overall, fiber orientation is the dominant factor governing fatigue strength, whereas frequency primarily affects the magnitude not the rate of fatigue degradation. These insights are valuable for designing Kevlar-reinforced composites for structural applications requiring reliable performance under cyclic loading.

NOMENCLATURE

Symbol	Description	Symbol	Description
A	Fatigue strength coefficient obtained from Basquin's law, MPa	UTS	Ultimate tensile strength obtained from static tensile testing, MPa
A_{norm}	Normalized fatigue strength coefficient (A/UTS)	β_0	Intercept in ANCOVA reduced model (reference level)
b	Basquin slope (fatigue exponent) obtained from log-log regression	β_1	Basquin slope in ANCOVA model (reference slope at 5 Hz)
c	Basquin intercept, equivalent to log(A) in Basquin's law	β_2	Intercept shift due to frequency (difference between 5 and 15 Hz)
CI	Confidence interval (95% unless specified)	β_3	Interaction term representing slope change due to frequency
E	Tensile modulus, GPa	ε	Mechanical strain, mm/mm
f	Loading frequency (5 Hz or 15 Hz), Hz	ϵ	Residual error term in ANCOVA/multivariate regression

LRR	Life Reduction Ratio between 5 Hz and 15 Hz fatigue lives	η^2	Partial eta-squared effect size (ANCOVA)
N	Number of cycles to failure, cycles	σ	Stress applied during tension-tension fatigue loading, MPa
R	Stress ratio (σ_{min} / σ_{max}) = 0.1	σ_{max}	Maximum cyclic stress for fatigue loading, MPa
R^2	Coefficient of determination for linear regression	σ_{min}	Minimum cyclic stress for fatigue loading, MPa
SE	Standard error of slope, intercept, or parameter estimate	σ / UTS	Normalized stress used for constructing normalized S–N curves

Credit Authorship Contribution Statement

Arzhang Faiq Mohammed: Conceptualization, Methodology, Experimental work, Data curation, Formal analysis, Writing – original draft, Writing – review & editing. Kareem Abdulghafour Abdulla: Supervision, Methodology, Validation, Reviewing, Project administration.

Declaration of Competing Interest

The authors declare that they have no known competing financial interests or personal relationships that could have appeared to influence the work reported in this paper.

REFERENCES

ASTM D3039/D3039M, 2008. Standard test method for tensile properties of polymer matrix composite materials*. ASTM International.*

ASTM D3479/D3479M, 2012. Standard test method for tension-tension fatigue of polymer matrix composite materials. ASTM International.

Ahmed, O. S., Aabid, A., Mohamed Ali, J. S., Hrairi, M., and Yatim, N. M., 2023. Progresses and challenges of composite laminates in thin-walled structures: A systematic review. *ACS Omega*, 8(34), pp. 30824–30837. https://doi.org/10.1021/acsomega.3c03695

Ansari, M. T. A., Singh, K. K., and Azam, M. S., 2022. Observations of fatigue damage development in woven glass fiber-reinforced polymer composite using transmission light photography technique. *Polymers and Polymer Composites*, 30, pp. 1–12. https://doi.org/10.1177/09673911221101300

Bannantine, J. A., Comer, J. J., and Handrock, J. L., 1990. *Fundamentals of Metal Fatigue Analysis*. Englewood Cliffs, New Jersey: Prentice Hall. ISBN: 0-13-340191-0.

Basquin, O., 1910. The exponential law of endurance tests*. Proceedings of the American Society for Testing Materials.* 10, pp. 625–630.

Bello, S., Agunsoye, J., Hassan, S., and Kana, M. Z., 2015. Epoxy resin-based composites, mechanical and tribological properties: A review. *Tribology in Industry*, 37(4), pp. 500–514.

Chowdhury, I. R., and Summerscales, J., 2024. Woven fabrics for composite reinforcement: A review. *Journal of Composites Science*, 8(7), P. 280. https://doi.org/10.3390/jcs8070280.

Cohen, J., 1988. *Statistical power analysis for the behavioral sciences* (2nd ed*.).* Lawrence Erlbaum Associates

Dehnad, M., Dolatabadi, M. K., Najafabadi, M. A., and Asgharian Jeddi, A. A., 2022. Behavior of woven fabric composite under tensile loads in different directions using acoustic emission. *Journal of Industrial Textiles,* P. 52. https://doi.org/10.1177/15280837221117611

Deng, H., Mochizuki, A., Fikry, M., Abe, S., Ogihara, S., and Koyanagi, J., 2022. Numerical and experimental studies for fatigue damage accumulation of CFRP cross-ply laminates based on entropy failure criterion. *Materials,* 16(1), P. 388. https://doi.org/10.3390/ma16010388

Islam, M. Z., and Ulven, C. A., 2022. Effect of loading frequency on the high cycle fatigue strength of flax fiber reinforced polymer matrix composites*. Journal of Renewable Materials*, 10(5), pp. 1185–1198.

Justo Estebaranz, J., Marín Vallejo, J. C., París Carballo, F., and Cañas Delgado, J., 2013. Study of the effect of frequency on composite laminates under uniaxial fatigue loads. *Composite Structures*, 100, pp. 317–325.

Kawai, M., and Taniguchi, T., 2006. Off-axis fatigue behavior of plain weave carbon/epoxy fabric laminates at room and high temperatures and its mechanical modeling. *Composites Part A: Applied Science and Manufacturing,* 37(2), pp. 243–256. https://doi.org/10.1016/j.compositesa.2005.07.003

Li, Z., Yang, Y., Cai, R., and Song, L., 2025. Off-axial tensile test and analysis for stratospheric airship envelope material. *Aerospace*, 12(4), pp. 1–12.

Liu, Y., Xie, J., Chen, X., Zhang, J., Wan, M., Sun, Z., and Yang, C., 2025. Characterization of progressive damage behaviour and failure mechanism of carbon fiber reinforced composite laminates*. Scientific Reports*, 15(1), P. 13791. https://doi.org/10.1038/s41598-025-98774-7

Ma, H., Bai, X., Ran, Y., Wei, X., and An, Z., 2022. Modeling the effect of stress ratio, loading frequency and fiber orientation on the fatigue response of composite materials. *Polymers*, 14(14), P. 2772. https://doi.org/10.3390/polym14142772

Marin, J., Justo, J., París, F., and Cañas, J., 2019. The effect of frequency on tension-tension fatigue behavior of unidirectional and woven fabric graphite-epoxy composites. *Mechanics of Advanced Materials and Structures*, 26(17), pp. 1430–1436. https://doi.org/10.1080/15376494.2018.1432814

Menail, Y., Mahi, A., and Assarar, M., 2015. Effect of fatigue testing and aquatic environment on the tensile properties of glass and Kevlar fibers reinforced epoxy composites. *Journal of Aeronautics & Aerospace Engineering*, 4(3), P. 1000150. https://doi.org/10.4172/2168-9792.1000150

Mohammadi, R., Assaad, M., Imran, A., and Fotouhi, M., 2024. Fractographic analysis of damage mechanisms dominated by delamination in composite laminates: A comprehensive review. *Polymer Testing*, 134, 108441. https://doi.org/10.1016/j.polymertesting.2024.108441

Montgomery, D. C., Peck, E. A., & Vining, G. G., 2021. *Introduction to Linear Regression Analysis*: John Wiley & Sons.

Obradović, V., Sejkot, P., Zabloudil, A., Machalická, K. V., and Vokáč, M., 2024. Degradation effect of moisture on mechanical properties of Kevlar/PVB composites with TiO_2 nanoparticles. *Buildings*, 14(2), P. 409. https://doi.org/10.3390/buildings14020409

Opelt, C., Cândido, G., and Rezende, M., 2018. Fractographic study of damage mechanisms in fiber reinforced polymer composites submitted to uniaxial compression. *Engineering Failure Analysis*, 92, pp. 520–527. https://doi.org/10.1016/j.engfailanal.2018.06.009

Prashanth, S., Subbaya, K., Nithin, K., and Sachhidananda, S., 2017. Fiber reinforced composites: A review. *Journal of Materials Science and Engineering*, 6(3), pp. 1–5.

Rajesh, S., Ramnath, B. V., Jayasooriya, M., and Ragavan, R., 2022. Review on mechanical characteristics of Kevlar composites. *Journal of Mines, Metals & Fuels*, 70(3), pp. 1–7.

Richardson, J. T., 2011. Eta squared and partial eta squared as measures of effect size in educational research. *Educational research review*, 6(2), pp. 135-147. https://doi.org/10.1016/j.edurev.2010.12.001

Reis, P. N., Silva, M. P., Santos, P., Parente, J., and Valvez, S., 2021. Effect of hostile solutions on the residual fatigue life of Kevlar/epoxy composites after impact loading. *Molecules*, 26(18), P. 5520. https://doi.org/10.3390/molecules26185520

Růžek, R., Kadlec, M., and Petrusová, L., 2018. Effect of fatigue loading rate on lifespan and temperature of tailored blank C/PPS thermoplastic composite. *International Journal of Fatigue*, 113, pp. 253–263. https://doi.org/10.1016/j.ijfatigue.2018.04.023

Salman, S. D., Sharba, M. J., Leman, Z., Sultan, M. T., Ishak, M. R., & Cardona, F., 2016. Tension–compression fatigue behavior of plain woven Kenaf/Kevlar hybrid composites. *Composite Structures*, 150, pp. 325–333.

Schulte, K., Reese, E., and Chou, T., 1987. Fatigue behaviour and damage development in woven fabric and hybrid fabric composites. *Proceedings of the Sixth International Conference on Composite Materials (ICCM-VI) and Second European Conference on Composite Materials (ECCM-II)*, pp. 1–10.

Shirinbayan, M., 2021. Multiscale damage analysis of the tension–tension fatigue behavior of a low-density sheet molding compound. *Journal of Applied Polymer Science*, 138(4), P. 49721. https://doi.org/10.1002/app.49721

Shirinbayan, M., Fitoussi, J., Meraghni, F., Surowiec, B., Laribi, M., and Tcharkhtchi, A., 2017. Coupled effect of loading frequency and amplitude on the fatigue behavior of advanced sheet molding compound (A-SMC). *Journal of Reinforced Plastics and Composites*, 36(4), pp. 271–282.

Shundo, A., Yamamoto, S., and Tanaka, K., 2022. Network formation and physical properties of epoxy resins for future practical applications. *JACS Au*, 2(7), pp. 1522–1542.

Suresh, S., 1998. *Fatigue of Materials* (2nd ed.). Cambridge: Cambridge University Press. https://doi.org/10.1017/CBO9780511806575

Tewani, H., Cyvas, J., Perez, K., and Prabhakar, P., 2025. Arχi-textile composites: Role of weave architecture on mode-I fracture energy in woven composites. *Composites Part A: Applied Science and Manufacturing,* 188, P. 108499. https://doi.org/10.1016/j.compositesa.2024.108499

Wickens, T. D., and Keppel, G., 2004. *Design and analysis: A researcher's handbook*, Vol. 860. Pearson Prentice-Hall Upper Saddle River, NJ.

Yang, Z., Yang, Y., Zheng, Z., and Shao, J., 2024. Study on fatigue damage and frequency attenuation characteristics of carbon fiber composite. *Composites and Advanced Materials*, 33, pp. 1–12. https://doi.org/10.1177/26349833241258784

Zhao, D., Wang, W., and Hou, Z., 2019. Tensile initial damage and final failure behaviors of glass plain-weave fabric composites in on- and off-axis directions. *Fibers and Polymers*, 20(1), pp. 147–157.

Zuo, P., Benevides, R. C., Laribi, M.-A., Fitoussi, J., Shirinbayan, M., Bakir, F., and Tcharkhtchi, A., 2018. Multi-scale analysis of the effect of loading conditions on monotonic and fatigue behavior of a glass fiber reinforced polyphenylene sulfide (PPS) composite. *Composites Part B: Engineering*, 145, pp. 173–181. https://doi.org/10.1016/j.compositesb.2018.03.020

الاعتماد على تردد التحميل في تعب الشد–شد لمركّب كيفلار/إيبوكسي المنسوج: منحنيات S–N المُطبَّعة ومعاملات باسكوين عند زوايا 0° و23° و45°

ئەرژەنگ فائق محمد*، كريم عبدالغفور عبدالله

قسم الهندسة الميكانيكية والميكاترونيكس، كلية الهندسة، جامعة صلاح الدين، اربيل،العراق

الخلاصة

في هذه الدراسة، تم فحص التأثير المشترك لكلٍّ من اتجاه الألياف وتردد التحميل على سلوك التعب من نوع الشد–شد لرقائق كيفلار/إيبوكسي المنسوجة. جرى تصنيع العينات عند زوايا توجيه ألياف مقدارها 0° و23° و45° باستخدام تقنية الرصّ اليدوي، كما تم اختبارها وفقًا للمواصفتين القياسيتين ASTM D3039 و ASTM D3479. وقد أظهرت اختبارات الشد السكوني، والتي بلغت فيها مقاومة الشد القصوى (UTS) قيمًا مقدارها 276.1 ميغاباسكال عند زاوية 0°، و159.2 ميغاباسكال عند زاوية 23°، و185.81 ميغاباسكال عند زاوية 45°، اعتمادًا واضحًا على اتجاه الألياف .تمت عملية تطبيع إجهادات التعب باستخدام النسبة (σ_max/UTS). كما أُجريت تجارب التعب عند مستويات إجهاد تراوحت بين 55% و90% من مقاومة الشد القصوى، وعند ترددين للتحميل هما 5 هرتز و15 هرتز . وتم تحليل النتائج وتفسيرها باستخدام منحنيات S–N المُطبَّعة، ونماذج انحدار باسكوين، وتحليل التباين المشترك(ANCOVA) ، ونسبة انخفاض العمر (LRR) ، إضافةً إلى التحليل المورفولوجي لأسطح الكسر باستخدام المجهر الإلكتروني الماسح .(SEM) أظهرت زيادة تردد التحميل انخفاضًا في أعمار التعب عند جميع زوايا التوجيه. فقد أبدت الرقاقة ذات الاتجاه 0° الأثر الأكثر اتساقًا للتردد، بمتوسط قيمة LRR قدره 0.446 (بفاصل ثقة 95% يتراوح بين 0.381 و0.511). وعلى النقيض من ذلك، أظهرت الرقائق عند زاويتي 23° و45° انخفاضات أقل وأكثر اعتمادًا على الإجهاد، حيث بلغ متوسط LRR نحو 0.186 (بفاصل ثقة 95% من 0.060 إلى 0.312) و0.162 (بفاصل ثقة 95% من 0.041 إلى 0.284)، على التوالي كما أظهرت نتائج تحليل ANCOVA عدم وجود فروق ذات دلالة إحصائية في ميل المنحنيات ناتجة عن اختلاف التردد ($p > 0.05$) عند أي من زوايا التوجيه، مما يشير إلى بقاء معدل تدهور عمر التعب دون تغيير. ومع ذلك، كانت تأثيرات مستوى التقاطع (intercept-level) ذات أهمية عملية واضحة عند زاويتي 0 (η^2 الجزئي = 0.313) و23 ° (η^2 الجزئي = 0.229)، وهو ما يعكس حدوث انخفاض يعتمد على التردد في مقاومة التعب .وقد دعمت مشاهدات المجهر الإلكتروني الماسح هذه النتائج، إذ لوحظت تشققات أوسع في المصفوفة وانسحاب أكبر للألياف عند الترددات الأعلى. وبوجهٍ عام، أظهرت رقائق كيفلار/إيبوكسي المنسوجة سلوك تعب متباين الخواص بشكل ملحوظ، حيث كان اتجاه الألياف العامل المسيطر، في حين كان تردد التحميل عاملًا ثانويًا إلا أنه ذو تأثير واضح.

الكلمات المفتاحية: اتجاه الألياف، سلوك الكلال، التردد، الكيفلر المنسوج.